Available online at www.sciencedirect.com
ScienceDirect
Trans. Nonferrous Met. Soc. China 35(2025) 460−473
Transactions of Nonferrous Metals Society of China
www.tnmsc.cn

Inhibition mechanism of NaF on WE43 Mg alloy in NaCl solution

Yun-tian YANG[1#], Yu-xin ZHOU[1#], Xiao-peng LU[1], Ji-rui MA[1], Jun-jie YANG[2,3], Fu-hui WANG[1]

1. State Key Laboratory of Digital Steel, Northeastern University, Shenyang 110819, China;
2. Institute of Advanced Wear & Corrosion Resistant and Functional Materials, Jinan University, Guangzhou 510632, China
3. Shaoguan Research Institute of Jinan University, Shaoguan 512027, China

Received 2 June 2023; accepted 4 March 2024

Abstract: The influence of NaF on the microstructure, composition and corrosion performance of WE43 Mg alloy in 3.5 wt.% NaCl solution was systematically investigated by means of SEM, TEM, EPMA, XRD, XPS and electrochemical measurements. It was proved that NaF is an effective inhibitor for WE43 Mg alloy and the highest inhibition efficiency is 92.6% at its concentration of 40 mmol/L in neutral NaCl solution. The dissolution of WE43 alloy is inhibited by formation and deposition of a dense and protective double-layered corrosion film by chemical reaction between corrosion inhibitor and dissolved Mg^{2+}. The microstructure and composition of this double-layered corrosion film were investigated by FIB and TEM. The outer layer of the corrosion film is found to be composed of $NaMgF_3$, MgF_2 and MgO, while the inner layer mainly consists of MgO and MgF_2.

Key words: Mg alloy; corrosion; corrosion film; inhibitor; inhibition mechanism

1 Introduction

Magnesium (Mg) has great potential as an engineering material for applications in industries due to its high specific strength [1−3]. Due to its biocompatibility and low density, Mg is utilized in the medical field [4−6]. In recent years, Mg has also been employed in the field of aqueous and secondary batteries due to the high conductivity and low cost [7−9]. Nevertheless, Mg alloy suffers severe corrosion attack due to its low standard potential (−2.37 V (vs SHE)) [10−13]. It was found that there is a large potential between the intermetallic phase and Mg matrix, promoting the micro-corrosion process [14,15]. Fe, Ni and other impurities inevitably enter the matrix during the smelting process, which further increase dissolution rate of the substrate [16−18]. Additionally, the corrosion film is primarily composed of $Mg(OH)_2$. The hydroxide layer is porous and has a minimal impact on limiting the corrosion process of the substrate [19−22]. Besides surface treatment processes, the introduction of corrosion inhibitors has been proved to be one of the most effective approaches to reduce the corrosion rate of Mg for industrial application [23−26]. It was reported that the adsorption of organic inhibitors onto the surface of Mg can greatly reduce the contact area between the matrix and electrolyte, leading to the enhanced corrosion resistance [27−30]. LU et al [31,32] found that sodium dodecyl sulfate (SDS) was adsorbed on the surface of AZ91 Mg alloy, which inhibited micro-galvanic corrosion and degradation process of the substrate. The inhibition efficiency of SDS on AZ91 Mg alloy was 88.8% after immersion

# Yun-tian YANG and Yu-xin ZHOU contributed equally to this work

Corresponding author: Xiao-peng LU, Tel: +86-13840388913, E-mail: luxiaopeng@mail.neu.edu.cn;
Jun-jie YANG, Tel: +86-15547287612, E-mail: junjieyang0612@gmail.com

DOI: https://doi.org/10.1016/S1003-6326(24)66692-6

for 48 h. YANG et al [33] studied the inhibition mechanism of carboxylic acids (2,5-PDCA and fumaric acid) on pure Mg. It was found that the adsorption of 2,5-PDCA and fumaric acid reduced the potential difference between the matrix and the secondary phase, which inhibited the micro-galvanic corrosion. XIAO et al [34] proved that sodium lignosulfonate (SLS) had a good corrosion inhibition effect on AZ31 Mg alloy and found that the adsorption of inhibitor on the sample surface was in line with Langmuir adsorption model. DINODI and SHETTY [35] found that the inhibition efficiency of 3 mmol/L stearate on ZE41 Mg alloy reached 88%. A compact and protective corrosion film was formed due to precipitation of adsorbed alkyl carboxylates on Mg alloy surface.

It was also found that inhibitors participate in the deposition of protective corrosion film on the sample surface by chemical reaction, which effectively influence the degradation process of the substrate [36−39]. POKHAREL et al [40] studied the influence of glycine on the corrosion performance of AZ31 Mg alloy in simulated body fluids. It was proved that glycine chelated with Ca^{2+} and deposited on Mg alloy surface after long-term immersion. KHARITONOV et al [41] found that 100 mmol/L Na_2MoO_4 had significant corrosion inhibition effect on WE43 Mg alloy. MoO_4^{2-} leads to the formation of $MoO(OH)_3$, which inhibits the dissolution process. PRINCE et al [42] concluded that passive film layer generated on AZ31 Mg alloy in the presence of 50 mmol/L Na_2CO_3. After 7 d of immersion, 80% of inhibition efficiency was achieved in this solution. HUANG et al [43] studied the synergistic effect of Na_3PO_4 and sodium dodecyl benzene-sulfonic acid (SDBS) on GW103 Mg alloy. The chemical reaction between Na_3PO_4 and Mg matrix resulted in the deposition of large amounts of $Mg_3(PO_4)_2$ on the sample surface, which greatly improved the protective ability of the corrosion product layer. QIU et al [44] found that 94.1% of inhibition efficiency was achieved by using NaF and DL-malic acid as inhibitor in NaCl solution. In the presence of mixed inorganic and organic inhibitor, large cubic $NaMgF_3$ particles were transformed into smaller and refined spheroidal particles, leading to superior corrosion performance.

In this work, NaF was selected as corrosion inhibitor to modify the degradation process and improve the corrosion resistance of WE43 Mg alloy. The inhibition mechanism of NaF on WE43 Mg alloy was studied by means of analyzing the composition and microstructure of the corrosion film layer formed on the sample surface.

2 Experimental

2.1 Material and reagents

WE43 Mg alloy was used and cut (10 mm × 10 mm × 5 mm) as the substrate. The Mg alloy samples were ground by emery papers before performing electrochemical corrosion tests. Different concentrations of NaF solution (5, 40 and 80 mmol/L) were added into 3.5 wt.% NaCl solution to study the influence of inhibitor on Mg alloy. pH value of all electrolytes was adjusted to 6.8−7.2 by dropping diluted NaOH solution. The chemicals used in this study were provided by Sinopharm Chemical Reagent Company in analytical grade.

2.2 Electrochemical measurements

The electrochemical corrosion tests were measured in conventional three-electrode cell by using Princeton Instruments P4000 (Ametek, the United States). 1 cm^2 of WE43 Mg alloy was used as the working electrode, a saturated calomel electrode was used as the reference electrode, and a platinum sheet was used as the counter electrode. The open circuit potential (OCP) was measured for 1 h to achieve a steady state before corrosion measurements. The polarization curves were collected from −300 mV (vs OCP) until anodic current density reached 10 mA/cm^2 with a scanning rate of 0.333 mV/s. The corrosion current density of sample was calculated by Stern equation (Eq. (1)). J_{corr} is the corrosion current density, β_a represents anodic polarization slope, β_c presents cathodic polarization slope, and R_p is the polarization resistance.

$$J_{corr}=\frac{\beta_a \beta_c}{\beta_a+\beta_c}\cdot\frac{1}{R_p} \tag{1}$$

Let J_{corr} and J'_{corr} represent the corrosion current density of the samples in the blank and NaF-containing NaCl solutions, respectively. The inhibition efficiency (η) was calculated based on Eq. (1) as follows:

$$\eta = \frac{J_{corr} - J'_{corr}}{J_{corr}} \times 100\% \tag{2}$$

The electrochemical impedance spectroscopy (EIS) measurement was performed with AC amplitude 10 mV sinusoidal perturbation in frequency range from 10^{-2} to 10^5 Hz. The obtained EIS data were fitted using a ZsimpWin software. All the measurements were repeated at least three times to ensure reproducibility.

2.3 Microstructure and elemental composition measurements

The surface and cross-sectional morphologies of the corroded samples after immersion test for 72 h were studied by scanning electron microscope (SEM, JSM−7001 F, JEOL, Japan). The phase composition of corrosion products was determined by using X-ray diffraction (Smartlab, Rigaku, Japan) in 2θ range from 15° to 80° with a scan rate of 4 (°)/min. X-ray photoelectron spectroscopy (Shimazu-Kratos Analytical, UK) was used to investigate the chemical composition of the corroded samples. Peak identification was performed using XPSpeak41 software as reference and the binding energy scale was calibrated to the C 1s peak (284.6 eV). The elemental composition and distribution of the corroded samples were investigated by electron probe microanalysis (EPMA, JXA−8530F JEOL, Japan). The microstructure and composition of the corrosion product layer after immersion for 72 h with addition of NaF were obtained by transmission electron microscopy (TEM, JEM−2100 F, Japan, 200 keV) to study the inhibition mechanism of the inhibitors. The TEM lamellae were milled from the corroded specimen with focused ion beam (FIB, Zeiss Crossbeam 350, Germany).

3 Results

3.1 Mass loss test

Mass loss test was carried out to study the influence of NaF concentrations on the corrosion behavior of Mg alloy in different solutions (Fig. 1). The addition of different concentrations of NaF reduces dissolution rate of the Mg alloy samples. After introduction of 40 mmol/L NaF into the electrolyte, the mass loss rate of the substrate is reduced to the lowest value (0.013 mm/a, 1 a= 1 year). As a result, the highest inhibition efficiency is found to be 87.37% after immersion for 72 h. It can be inferred that addition of NaF might contribute to deposition of corrosion product layer with enhanced barrier property, which effectively inhibits the degradation process of Mg alloy.

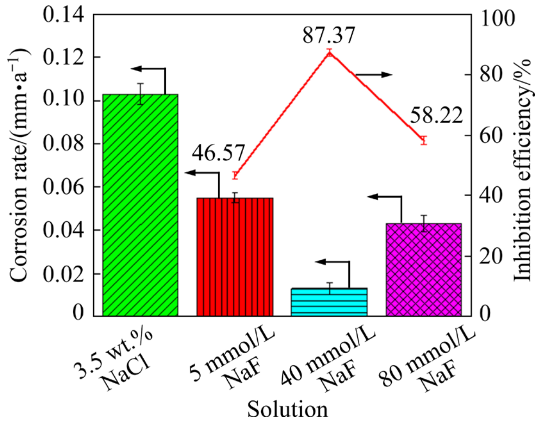

Fig. 1 Corrosion rate and inhibition efficiency of WE43 Mg alloy after immersion in various solutions for 72 h

3.2 Electrochemical behavior

3.2.1 Electrochemical impedance spectroscopy

Figure 2 demonstrates the EIS data of sample immersed in different electrolytes. WE43 Mg alloy displays relatively low corrosion resistance during the immersion in 3.5 wt.% NaCl solution. The impedance of the sample starts to decrease after immersion for 24 h and an inductive loop appears since the beginning of the EIS measurement. Obviously, the presence of different concentrations of inhibitor significantly enhances the corrosion performance of the substrate. The sample shows the largest capacitive loop in the presence of 40 mmol/L NaF after soaking in the electrolyte for 72 h. The impedance value at low frequency sharply increases from 611.2 Ω·cm^2 (blank NaCl solution) to 5091 Ω·cm^2 (Table 1), suggesting that the protective capability of the corrosion product layer is greatly enhanced. As demonstrated in Table 1 and Fig. 3, R_s represents the solution resistance; R_f and CPE$_f$ are related to the corrosion resistance and capacitance of the corrosion film formed on sample surface, respectively; R_{ct} corresponds to the charge transfer resistance, while CPE$_{dl}$ is the capacitance of double layer at metal/electrolyte interface. The evolution of R_p (R_{ct}+R_f) during immersion in different solutions is depicted in Fig. 3(b). The impedance of the samples immersed in 5 and 80 mmol/L NaF containing electrolyte increases firstly and decreases after 48 h

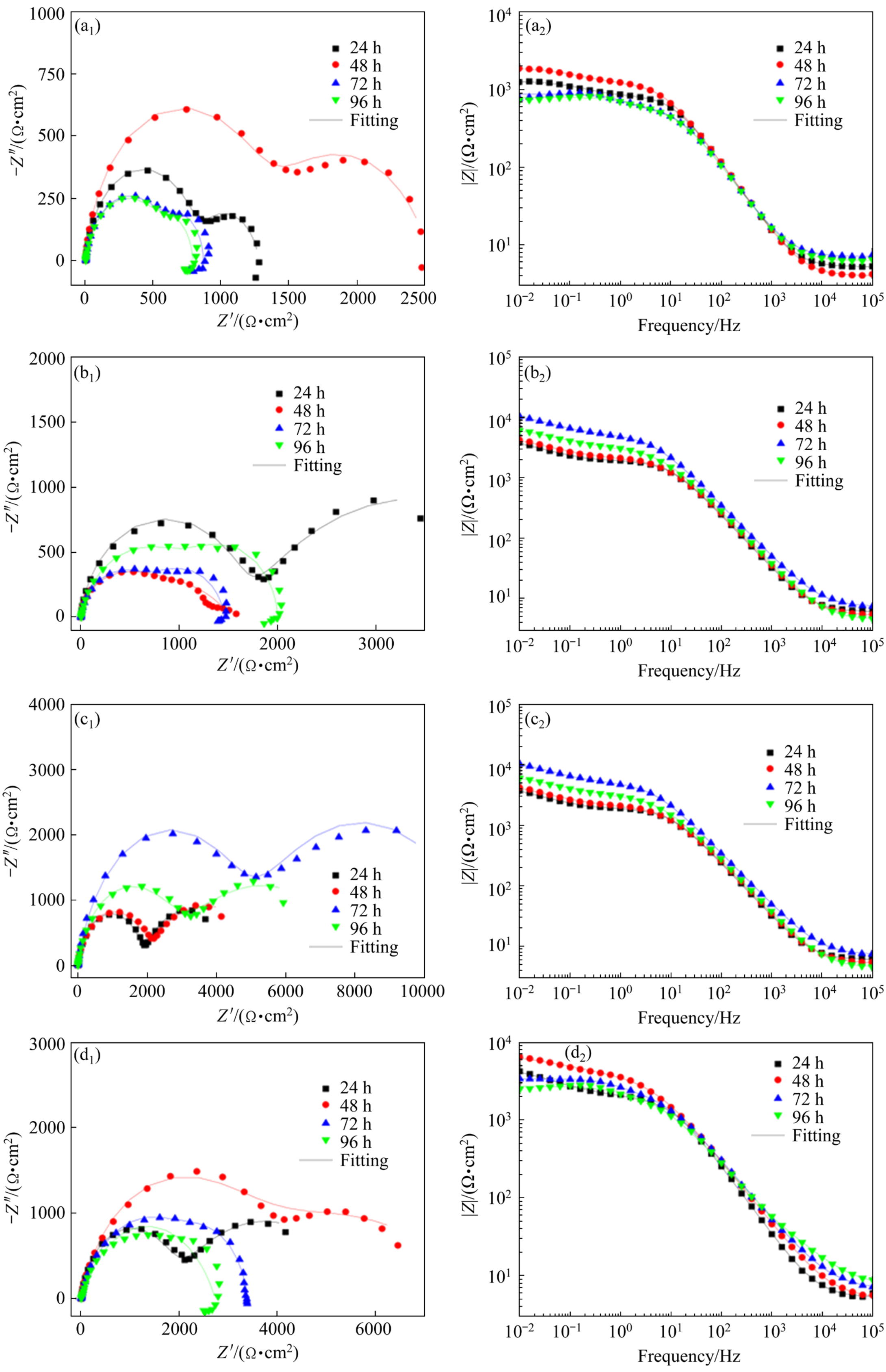

Fig. 2 Electrochemical impedance spectra and fitting curves for WE43 Mg alloy immersed in 3.5 wt.% NaCl (a_1, a_2), 3.5 wt.% NaCl + 5 mmol/L NaF (b_1, b_2), 3.5 wt.% NaCl + 40 mmol/L NaF (c_1, c_2), and 3.5 wt.% NaCl + 80 mmol/L NaF (d_1, d_2) solutions for different time

Table 1 Fitted results of impedance spectra

Solution	Time/h	R_s/(Ω·cm^2)	CPE$_f$/(μS·s^{-n}·cm^{-2})	n_1	R_f/(Ω·cm^2)	CPE$_{dl}$/(μS·s^{-n}·cm^{-2})	n_2	R_{ct}/(Ω·cm^2)
3.5 wt.% NaCl	24	5.2	23.43	0.92	838.8	2384	0.82	437.9
	48	5.16	27.09	0.90	991.8	1869	0.74	810.7
	72	7.04	31.11	0.88	611.2	597.1	0.95	255.8
	96	6.17	30.94	0.88	598.8	546.8	0.92	188.7
3.5 wt.% NaCl + 5 mmol/L NaF	24	5.84	12.74	0.92	1677	1851	0.61	3474
	48	5.15	14.62	0.92	595.2	406.8	0.51	934.8
	72	5.78	16.92	0.90	817.2	245.4	0.88	644.7
	96	8.12	25.23	0.87	1300	250.9	0.90	700.8
3.5 wt.% NaCl + 40 mmol/L NaF	24	5.98	13.18	0.89	1883	1890	0.74	2554
	48	5.25	13.54	0.88	1952	1149	0.60	3543
	72	7.28	11.36	0.86	5091	548.5	0.70	6673
	96	4.43	13.2	0.87	2791	638.1	0.53	5324
3.5 wt.% NaCl + 80 mmol/L NaF	24	5.28	12.88	0.89	1907	1008	0.56	3734
	48	5.11	17.66	0.81	3256	431.5	0.43	4837
	72	6.65	21.86	0.77	2674	229.5	0.91	724.1
	96	7.05	35.29	0.69	171.4	0.68	0.95	2556

n_1 and n_2 are indexes ranging from 0 to 1, determining whether CPE$_f$ or CPE$_{dl}$ behaves as resistance (n_1 or n_2=0) or capacitance (n_1 or n_2=1)

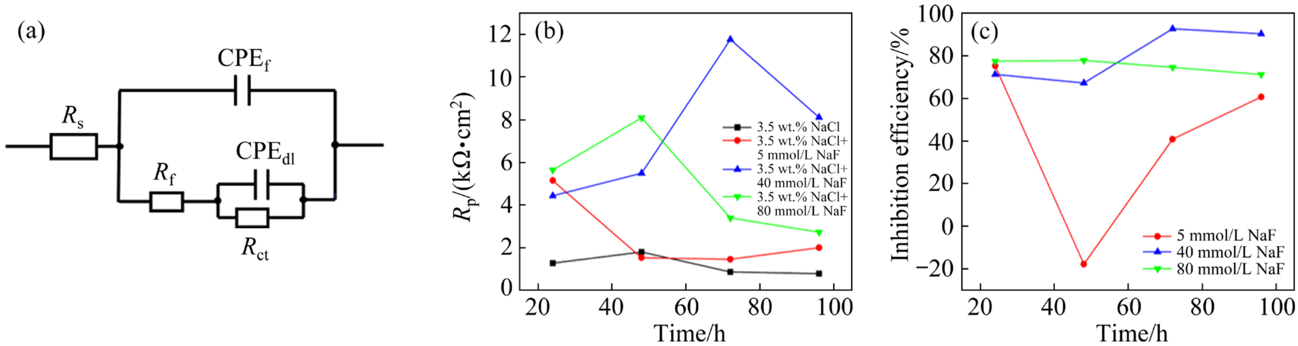

Fig. 3 Equivalent circuit used to fit EIS data (a), evolution of R_p during immersion in various solutions (b), and inhibition efficiency of different concentrations of NaF solutions (c)

immersion. In contrast, the addition of 40 mmol/L NaF into the electrolyte demonstrates the highest corrosion resistance during the entire corrosion test. R_p of the sample is found to be 11764 Ω·cm^2 after EIS test for 72 h, which is more than 10 times compared to that in the blank electrolyte. The evolution of the inhibition efficiency during EIS measurement can be found in Fig. 3(c). It is clear that the inhibition efficiency of NaF increases with the increase of its concentration in the electrolyte.

3.2.2 Open circuit potential and polarization curves

The evolution of OCP and polarization curves of Mg samples after immersion in various solutions for different time is shown in Fig. 4. It is observable that the OCP of the Mg alloy sample surface is reduced when immersed in the electrolyte in the presence of high concentration of inhibitor. This might be related to the dissolution and precipitation of corrosion products on the sample surface during corrosion test. In terms of blank electrolyte, the anodic branch of the polarized sample firstly moves to the left direction after immersion for 24 h and subsequently shifts to the right side until 96 h, indicating that the substrate degrades continually with the increase of immersion time. For samples immersed in inhibitor-containing solution, the anodic branch of the curves seems to show a passivation region after certain immersion time,

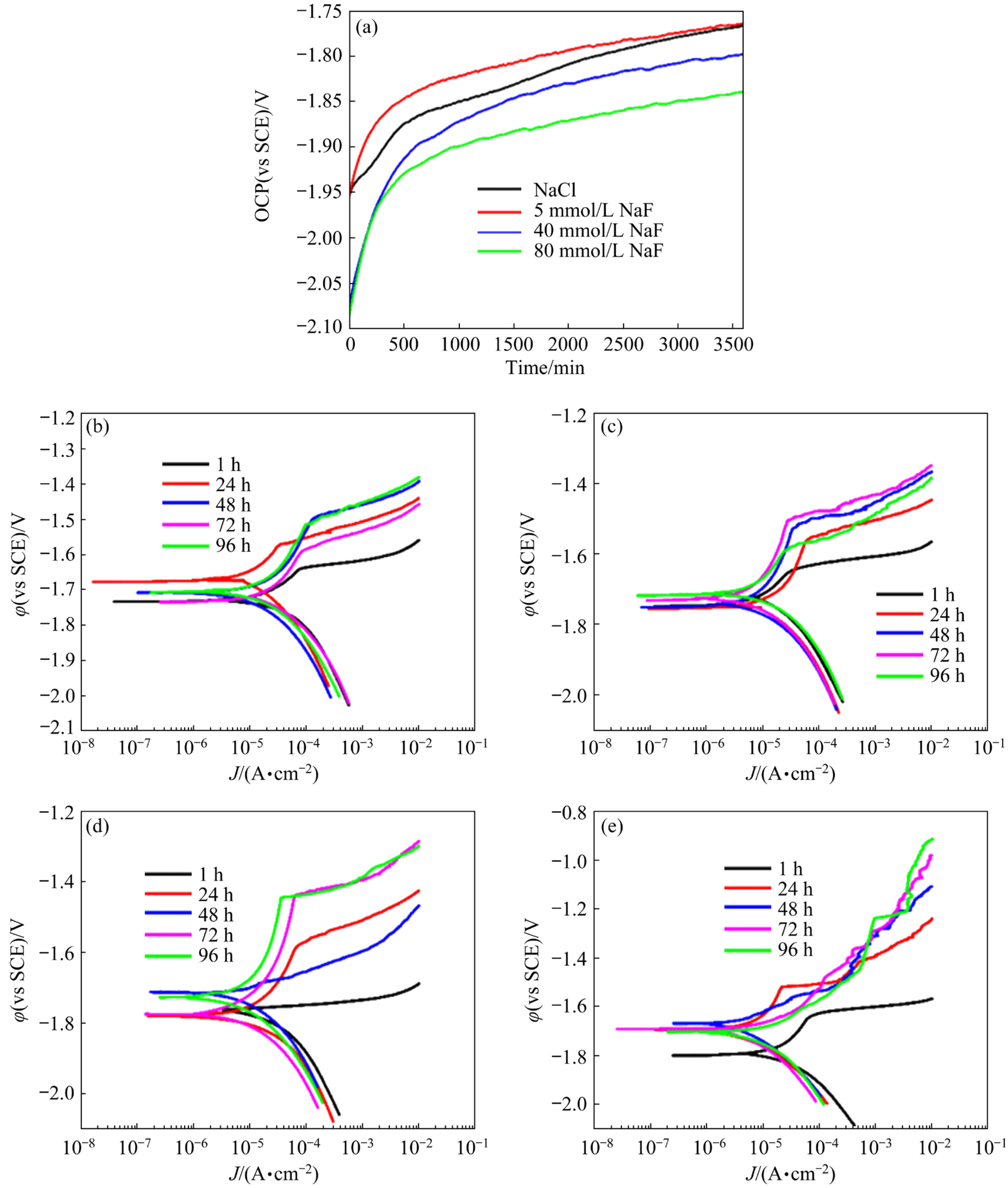

Fig. 4 Evolution of OCP of samples during immersion in different solutions (a), and polarization curves of Mg alloy after immersion for different time in 3.5 wt.% NaCl (b), 3.5 wt.% NaCl + 5 mmol/L NaF (c), 3.5 wt.% NaCl + 40 mmol/L NaF (d), and 3.5 wt.% NaCl + 80 mmol/L NaF (e) solutions

indicating that the anodic dissolution kinetics is suppressed in the presence of NaF. The corrosion potential (φ_{corr}) and corrosion current density (J_{corr}) of different samples were calculated from the cathodic polarization branch, as shown in Table 2. It can be found that higher concentration of inhibitor in the electrolyte results in lower corrosion current density and the sample after immersion in 40 mmol/L inhibitor-containing solution for 72 h demonstrates the lowest J_{corr} (8.49 μA/cm^2). The abovementioned results suggest that the presence of NaF facilitates the formation of corrosion product layer with enhanced barrier property on the sample surface.

Table 2 Corrosion performance of WE43 Mg alloy immersed in different solutions

Solution	Time/h	φ_{corr} (vs SCE)/V	J_{corr}/(A·cm^{-2})
3.5 wt.% NaCl	1	−1.73	4.42×10^{-5}
	24	−1.67	1.41×10^{-5}
	48	−1.71	1.24×10^{-5}
	72	−1.72	2.90×10^{-5}
	96	−1.70	1.44×10^{-5}
3.5 wt.% NaCl + 5 mmol/L NaF	1	−1.76	3.01×10^{-5}
	24	−1.78	1.22×10^{-5}
	48	−1.71	2.25×10^{-5}
	72	−1.77	1.24×10^{-5}
	96	−1.73	1.16×10^{-5}
3.5 wt.% NaCl + 40 mmol/L NaF	1	−1.72	1.50×10^{-5}
	24	−1.75	1.57×10^{-5}
	48	−1.74	1.00×10^{-5}
	72	−1.73	8.49×10^{-6}
	96	−1.71	1.27×10^{-5}
3.5 wt.% NaCl + 80 mmol/L NaF	1	−1.79	2.83×10^{-5}
	24	−1.70	1.13×10^{-5}
	48	−1.67	8.99×10^{-6}
	72	−1.69	1.01×10^{-5}
	96	−1.70	1.23×10^{-5}

3.3 Characteristics of corroded samples

3.3.1 Surface and cross-section morphologies

According to the electrochemical corrosion tests, the sample demonstrates superior corrosion performance in the presence of 40 mmol/L NaF. Therefore, the microstructure and composition of such corroded sample are investigated to further study the inhibition mechanism of NaF in NaCl solution, as shown in Fig. 5. After being immersed in 3.5 wt.% NaCl solution for 72 h (Fig. 5(a)), apparent corrosion products and large cracks can be observed on the sample surface. In terms of the cross-sectional morphology, the corrosion product layer is non-uniform and porous. Large chunks of corrosion products are found to be adjacent to the intermetallic phase (Fig. 5(b)), indicating that the matrix is preferentially dissolved due to micro-galvanic corrosion effect. It can be inferred that such a corrosion layer is not capable of providing sufficient protection for the substrate. As for the sample immersed in inhibitor-containing solution, a thick and dense corrosion product layer can be clearly visible on the Mg alloy surface (Figs. 5(c) and (d)). In particular, large and irregular particles are found on the sample surface, suggesting that large amounts of corrosion products are formed and deposited during immersion test.

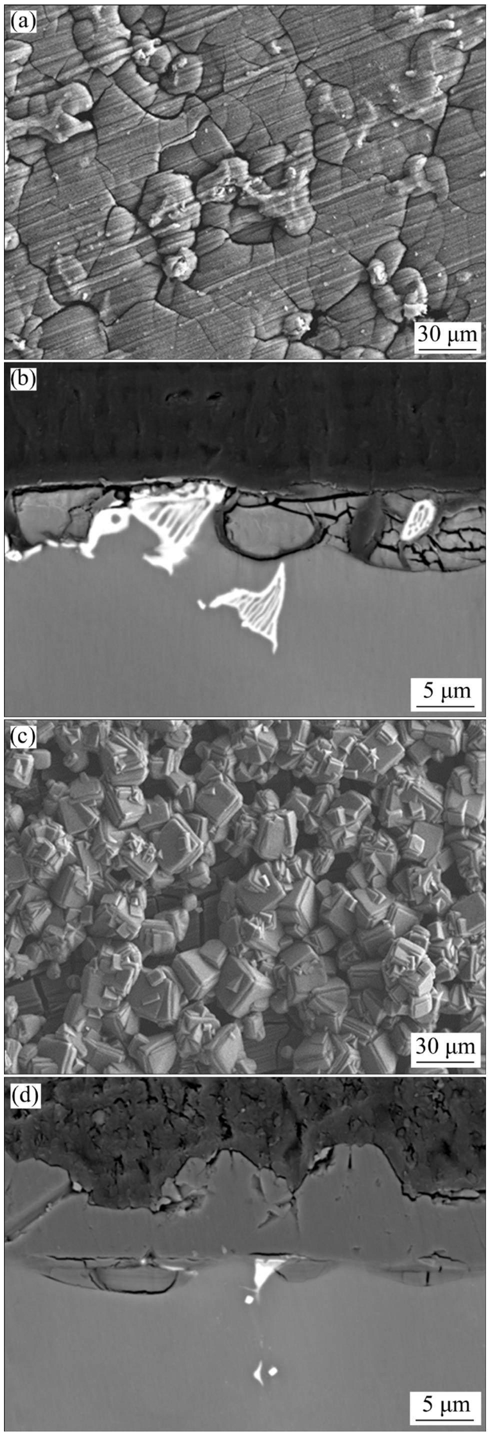

Fig. 5 SEM images of Mg alloy after immersion in 3.5 wt.% NaCl (a, b) and 3.5 wt.% NaCl + 40 mmol/L NaF (c, d) solutions for 72 h

3.3.2 Composition of corroded samples

EPMA is used to study the elemental distribution and composition of corroded samples after being immersed in NaF-containing electrolyte. Different colors are employed to present various kinds of elements. Compared to dark places, the bright places indicate high density for each element. Figure 6(a) shows that the corrosion product layer

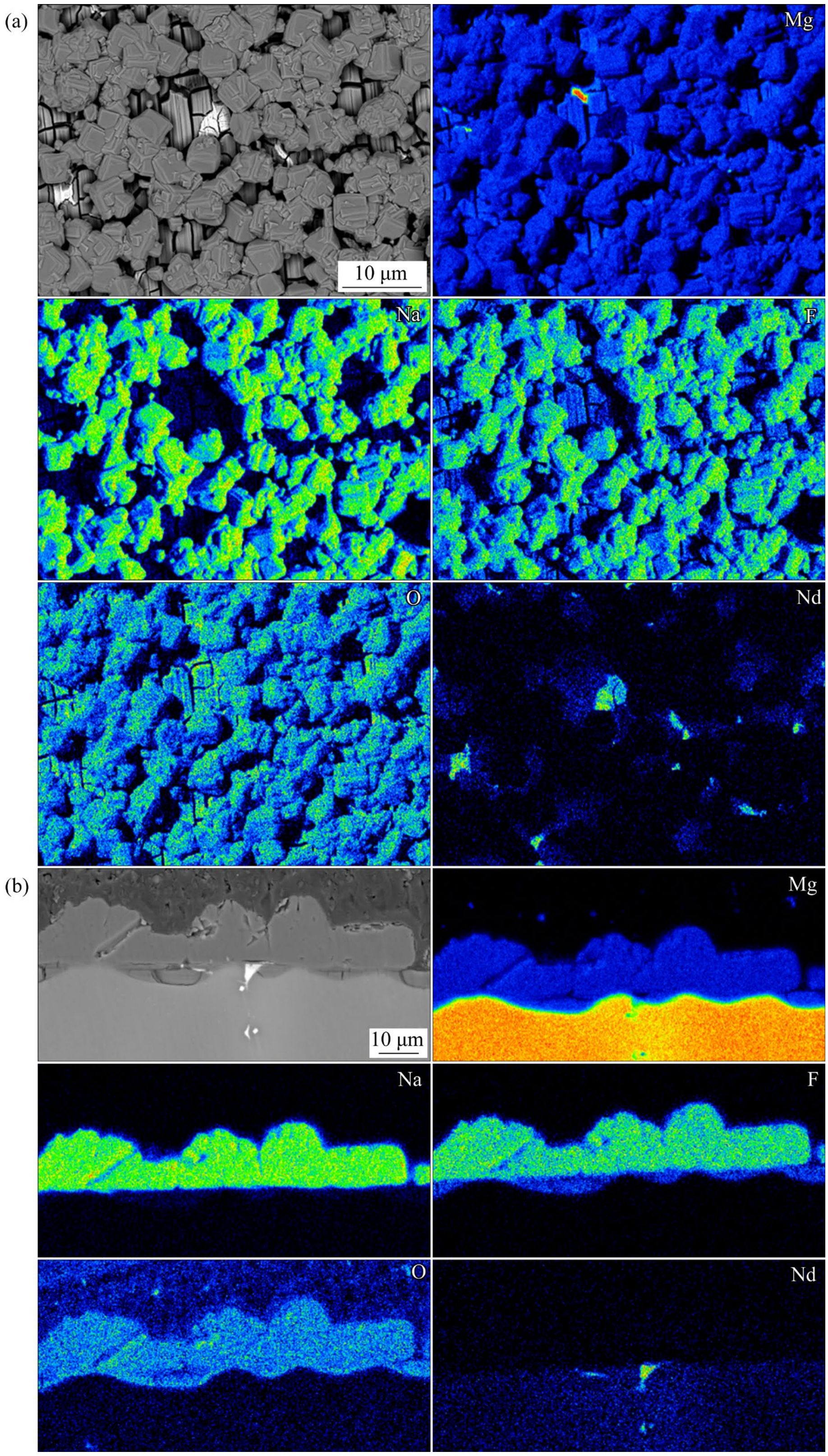

Fig. 6 EPMA mappings of surface (a) and cross-section (b) of corroded sample after immersion in 3.5 wt.% NaCl + 40 mmol/L NaF solution for 72 h

is divided into two sub-layers. The main elements of the corrosion products are O, Mg, F and Na. The outer corrosion layer has large-sized and irregular corrosion products, while the inner layer seems to be denser with some cracks (Fig. 6(a)). In terms of chemical composition, Mg, Na, F and O can be detected in the outer corrosion product layer. As for the inner corrosion layer, Na is not detectable and the content of F is less than that in the outer layer. The bright particles underneath are most likely to be rare earth-containing secondary phase. Figure 6(b) demonstrates the elemental composition and distribution of the cross-section. A clear boundary can be found between the inner and outer corrosion layers. The distribution of the main elements in the cross-section of the corroded sample is consistent with the surface morphology. In other words, the composition of the corrosion products varies in the outer and inner corrosion films. Moreover, the inner layer appears to be denser and thinner in contrast with the outer corrosion layer.

Figure 7 displays the XRD patterns of the corroded samples. The main corrosion product of samples is $Mg(OH)_2$ after being immersed in the blank solution. However, $Mg(OH)_2$ phase is hardly to be detected in samples with the addition of corrosion inhibitor. It should be noticed that $NaMgF_3$, MgF_2 and small amount of MgO are detected in the corrosion product layer after soaking in NaF containing solution for 72 h, indicating that the inhibitor is involved in the formation and deposition of corrosion products.

The composition of the corroded sample is also measured by using the X-ray photoelectron spectroscopy (XPS), as shown in Fig. 8. In the XPS

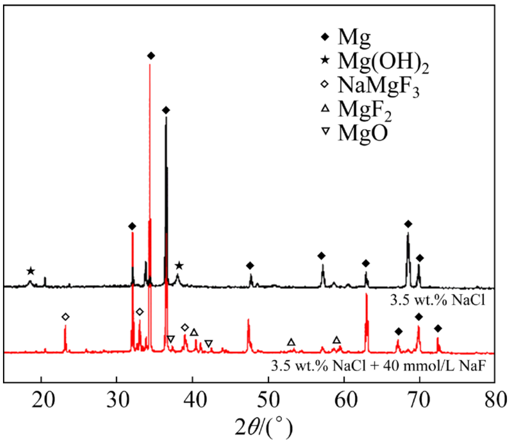

Fig. 7 XRD patterns of corroded samples immersed in 3.5 wt.% NaCl (a) and 3.5 wt.% NaCl + 40 mmol/L NaF (b) solutions

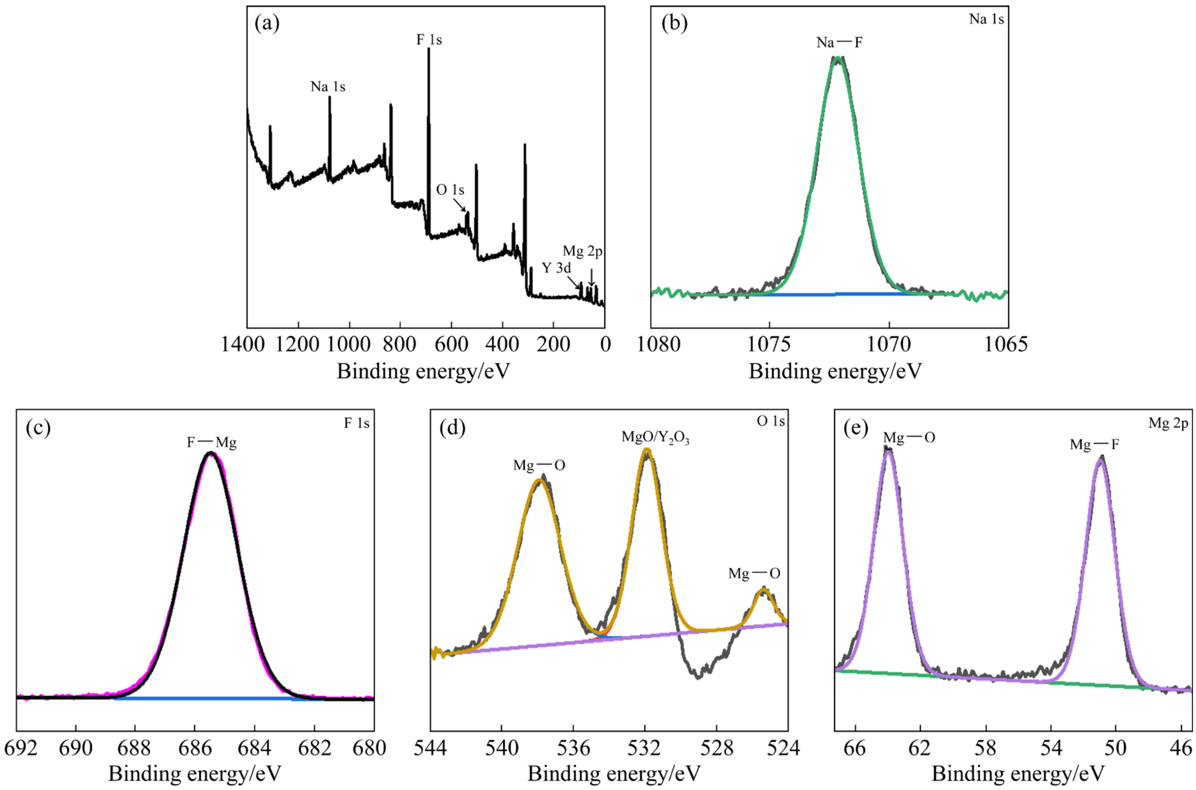

Fig. 8 XPS (a) and high-resolution (b−e) spectra of sample after immersion in 3.5 wt.% NaCl + 40 mmol/L NaF solution for 72 h

spectra of Na 1s and F 1s, peaks at 1072.2 and 685.5 eV are related to Na—F and F—Mg bonds, which can be associated with the presence of $NaMgF_3$ and MgF_2, respectively. O 1s spectrum at 538.1, 531.9 and 525.8 eV is related to MgO and Y_2O_3. The Mg 2p spectrum can be fitted by two peaks at 50.9 and 63.9 eV, which represents F—Mg and MgO, respectively.

FIB and TEM tests are used to further investigate the microstructure and composition of the corrosion film with the addition of inhibitor. The corrosion product on top of α-Mg is cut by means of FIB (Fig. 9(a)). The corrosion product layer is composed of two layers and a large crack is observed between the outer and inner corrosion layers. In addition, an ultrathin layer can be detected at the interface between Mg substrate and the inner corrosion layer, as shown in Fig. 9(b). Figure 10 shows the SAED ring and diffraction results of the selected regions in the corrosion product layer. It is apparent that the addition of NaF into the NaCl solution suppresses the formation and deposition of $Mg(OH)_2$. The phase composition of the outer corrosion layer has been identified to be $NaMgF_3$, MgF_2 and MgO. As for the inner corrosion layer, it mainly consists of MgF_2 and MgO. Additionally, MgO is found to be the main composition at the interface between Mg substrate and corrosion product layer.

4 Discussion

The corrosion behavior of WE43 Mg alloy is greatly influenced after the addition of NaF into

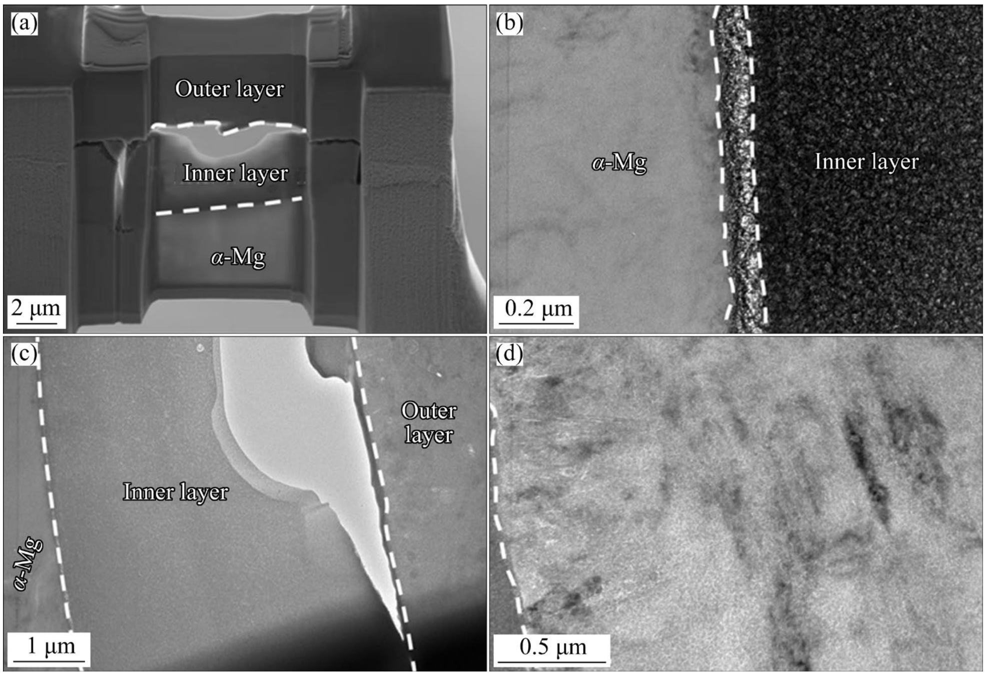

Fig. 9 Overview TEM image of corrosion layer after FIB milling (a), and TEM images of corrosion product on top of α-Mg (b−d)

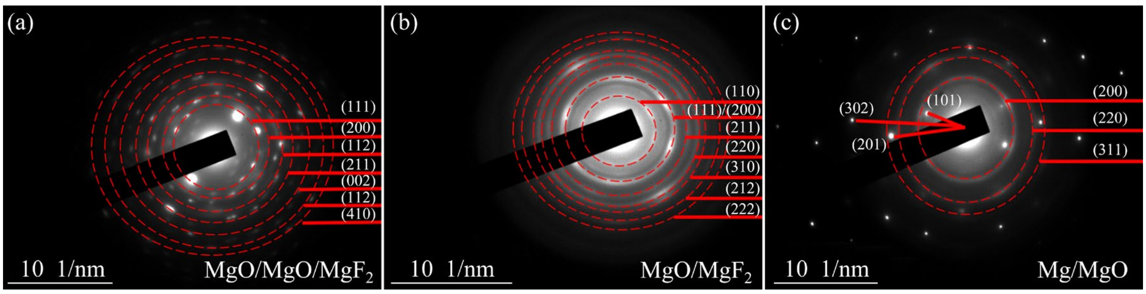

Fig. 10 SAED ring and diffraction results of corrosion products in different regions: (a) Interface layer in Fig. 9(b); (b) Inner corrosion layer in Fig. 9(c); (c) Outer corrosion layer in Fig. 9(d)

NaCl solution. On the one hand, the presence of NaF can suppress the formation of $Mg(OH)_2$ compared to the blank NaCl solution, which will in turn increase the densification of the corrosion film. The effect of inhibitor on the corrosion products is analyzed by using Hydra−Medusa software, as demonstrated in Fig. 11. It is clear that the formation and deposition of $Mg(OH)_2$ are inhibited in the presence of NaF. According to Fig. 11(b), the final pH of the electrolyte after performing corrosion test is 9.84, while formation of insoluble $Mg(OH)_2$ occurs when pH is 11.14. On the other hand, the addition of inhibitor into the electrolyte contributes to the deposition of a dense and thick corrosion product layer, which becomes a barrier to improve the corrosion resistance of the substrate.

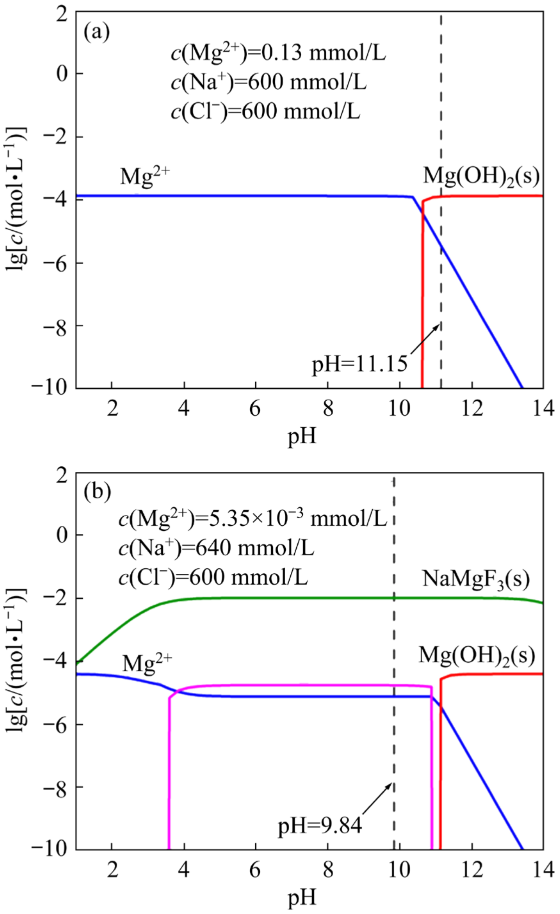

Fig. 11 Thermodynamic calculation of equilibrium composition of Mg alloy immersed in different electrolytes: (a) 3.5 wt.% NaCl solution; (b) 3.5 wt.% NaCl + 40 mmol/L NaF solution

As demonstrated by Figs. 6−11, the main composition of the corrosion products consists of $NaMgF_3$, MgF_2 and MgO. The formation of MgF_2 and $NaMgF_3$ can be explained by the following two reactions:

$$Mg^{2+}+2F^{-}=MgF_2(s) \qquad (3)$$

$$MgF_2(s)+F^{-}+Na^{+}=NaMgF_3(s) \qquad (4)$$

Since the solubility of MgF_2 (K_{sp}=5.16×10^{-11}, 25 °C) is significantly larger compared to that of $Mg(OH)_2$ (K_{sp}=5.61×10^{-12}, 25 °C), the dissolved Mg^{2+} ions preferentially react with F^-, which deposit directly on the Mg alloy surface. Afterwards, a large amounts of F^- and Na^+ in the electrolyte will further take part in the formation and deposition of corrosion product, as verified by the appearance of $NaMgF_3$ in the outermost layer of the corroded sample. Therefore, the presence of NaF facilitates the formation and deposition of stable and dense corrosion product layer on top of Mg alloy, and the inhibition efficiency is mainly related to the corrosion resistance of the inner barrier layer.

5 Conclusions

(1) NaF is an effective inhibitor for WE43 Mg alloy in 3.5 wt.% NaCl solution. After immersion in 40 mmol/L NaF containing solution, the highest inhibition efficiency of the inhibitor is found to be 92.6%.

(2) The formation and deposition of $Mg(OH)_2$ are suppressed after the addition of NaF, as the inhibitor contributes to the deposition of a double-layered corrosion product film on the sample surface.

(3) The inner layer appears to be thinner but denser compared to the outer corrosion layer. The main composition of the inner corrosion layer is MgO and MgF_2, which plays a key role in providing barrier property for the substrate.

(4) The outer corrosion layer consists of $NaMgF_3$, MgF_2 and MgO, which is porous and thicker compared to the inner layer.

CRediT authorship contribution statement

Yun-tian YANG and **Yu-xin ZHOU:** Conceptualization, Methodology, Investigation, Writing − Original draft preparation; **Xiao-peng LU:** Conceptualization, Investigation, Writing − Reviewing and editing, Supervision, Funding acquisition; **Ji-rui MA:** Conceptualization, Writing − Reviewing and editing; **Jun-jie YANG:** Investigation, Supervision, Writing − Reviewing and editing; **Fu-hui WANG:** Conceptualization, Writing − Reviewing and editing, Supervision, Funding acquisition.

Declaration of competing interest

The authors declare that they have no known competing financial interests or personal relationships that could have appeared to influence the work reported in this paper.

Acknowledgments

The authors would like to acknowledge the financial supports from the National Natural Science Foundation of China (No. 52071067), Liaoning Revitalization Talents Program, China (No. XLYC2403026), the Shenyang Young and Middle-aged Science and Technology Innovation Talent Support Program of China (No. RC231178), the Natural Science Foundation Project of Liaoning Province, China (No. 2022-YGJC-16), and the Fundamental Research Funds for the Central Universities, China (No. N2302019). Jun-jie YANG appreciates the financial supports by the National Natural Science Foundation of China (No. 52101084), Guangdong Basic and Applied Basic Research Foundation, China (No. 2023A1515011579), Guangzhou Basic and Applied Basic Research Foundation, China (No. 2024A04J9889), and the National Key Research and Development Project of China (No. 2023YFB3408200).

References

[1] WILLIAMS G, MCMURRAY H N, GRACE R. Inhibition of magnesium localised corrosion in chloride containing electrolyte [J]. Electrochimica Acta, 2010, 55(27): 7824−7833.

[2] CI Wen-jun, CHEN Xian-hua, SUN Yue, DAI Xu, ZHU Guan-zheng, ZHAO Di, PAN Fu-sheng. Effect of Zn on mechanical and corrosion properties of Mg−Sc−Zn alloys [J]. Journal of Materials Science & Technology, 2023, 158: 31−42.

[3] LI Zhao-xia, YANG Wen-bin, YU Qiang-liang, WU Yang, WANG Dao-ai, LIANG Jun, ZHOU Feng. New method for the corrosion resistance of AZ31 Mg alloy with a porous micro-arc oxidation membrane as an ionic corrosion inhibitor container [J]. Langmuir, 2019, 35(5): 1134−1145.

[4] KONG Jiu-chu, KOLOOSHANI A, KOLAHDOUZ A, NEJAD M G, TOGHRAIE D. Fabrication and characterization of magnesium implants coated with magnetic nanoparticles−wollastonite−hydroxyapatite for medical and sports injury applications: Finite element analysis [J]. Ceramics International, 2024, 50(3): 5755−5765.

[5] LI Yu-feng, WANG Bo-wen, SUN Xiao-hao, LIU De-bao. Effect of MgF_2 coating on stress corrosion cracking behavior of Mg−Zn−Ca alloy in simulated body fluid [J]. Transactions of Nonferrous Metals Society of China, 2023, 33(7): 2044−2053.

[6] ZHANG Zheng-yi, LU Sheng, LV Wei-gang, GU Jun-jie, ZHOU Shu-fan, ZHANG Jin-wei, OLEKSANDR D, WANG Ze-xin, CHEN Liang-yu. Enhanced corrosion resistance and biofunctionality of Zn−Al layered double hydroxide coating on micro-arc oxidized ZK60 Mg alloy via ion exchange [J]. Materials Chemistry and Physics, 2023, 299: 127482.

[7] LIU Yuan, SU Guang. Carbon and silicon nanotubes and carbon and silicon nanocages as anodes in Li-ion battery and Mg-ion battery [J]. Inorganic Chemistry Communications, 2024, 159: 111752.

[8] LING Ning, SONG Shan-shan, WANG Cai-li, FAN Hao-yuan, ZHANG Jing-lai, WANG Li. Novel dual-function electrolyte additive for high-power aqueous Mg−air battery: Improvement of both discharge potential and utilization efficiency [J]. Chemical Engineering Science, 2024, 285: 119624.

[9] LIU Zhou-lin, BAO Jia-xin, SHA Jian-chun, ZHANG Zhi-qiang. Modulation of the discharge and corrosion properties of aqueous Mg−air batteries by alloying from first-principles theory [J]. The Journal of Physical Chemistry C, 2023, 127(21):10062−10068.

[10] LIU Ze-qi, YANG Wen-lu, HE Xiao-xiao, CHENG Tian-cai, HUANG Hua-liang, XIONG Jing, HUANG Gang-liang. Synthesis of a green inhibitor and its inhibition behavior on AZ91D magnesium alloy in distilled water [J]. Surfaces and Interfaces, 2022, 30: 101870.

[11] LU Xiao-peng, MOHEDANO M, BLAWERT C, MATYKINA E, ARRABAL R, KAINER K U, ZHELUDKEVICH M L. Plasma electrolytic oxidation coatings with particle additions—A review [J]. Surface and Coatings Technology, 2016, 307: 1165−1182.

[12] ZHANG Chun-yan, LIAO Shang-ju, YU Bao-xing, LU Xiao-peng, CHEN Xiao-bo, ZHANG Tao, WANG Fu-hui. Ratio of total acidity to pH value of coating bath: A new strategy towards phosphate conversion coatings with optimized corrosion resistance for magnesium alloys [J]. Corrosion Science, 2019, 150: 279−295.

[13] ZHOU Yu-xin, LU Xiao-peng, YANG Lei, TIE Di, ZHANG Tao, WANG Fu-hui. Regulating discharge performance of Mg anode in primary Mg−air battery by complexing agents [J]. Electrochimica Acta, 2021, 370: 137805.

[14] LI Lin-xin, XIE Zhi-hui, FERNANDEZ C, WU Liang, CHENG Dao-jian, JIANG Xiao-hui, ZHONG Chuan-jian. Development of a thiophene derivative modified LDH coating for Mg alloy corrosion protection [J]. Electrochimica Acta, 2020, 330: 135186.

[15] MALEKI M, EMAMY M, DEHGHANIAN C, MIRZADEH H. On the solidification characteristics and corrosion resistance of in situ Mg–3Si–xCu composites [J]. Vacuum, 2022, 206: 111559.

[16] LI Chuan-qiang, TONG Zhi-pei, HE Yi-bin, HUANG Huai-pei, DONG Yong, ZHANG Peng. Comparison on corrosion resistance and surface film of pure Mg and Mg−14Li alloy [J]. Transactions of Nonferrous Metals Society of China, 2020, 30(9): 2413−2423.

[17] ZHANG Xin, Li Yong-jun, ZHANG Kui, WANG Chang-shun, LI Hong-wei, MA Ming-long, ZHANG Bao-dong. Corrosion and electrochemical behavior of Mg−Y alloys in 3.5% NaCl solution [J]. Transactions of Nonferrous Metals

Society of China, 2013, 23(5): 1226−1236.

[18] FENG Bao-jing, LIU Guo-nan, YANG Pei-xu, HUANG Sen-sen, QI Dong-qing, CHEN Peng, WANG Cheng-duo, DU Jiang, ZHANG Shao-jun, LIU Jin-hui. Different role of second phase in the micro-galvanic corrosion of WE43 Mg alloy in NaCl and Na_2SO_4 solution [J]. Journal of Magnesium and Alloys, 2022, 10(6): 1598−1608.

[19] LI Yi, LU Xiao-peng, MEI Di, ZHANG Tao, WANG Fu-hui. Passivation of corrosion product layer on AM50 Mg by corrosion inhibitor [J]. Journal of Magnesium and Alloys, 2022, 10(9): 2563−2573.

[20] XI Guo-qiang, MOU Yu, MA Yan-long, ZHAO Xu-han, XIONG Ju, MA Kai, WANG Jing-feng. Effect of volume fraction of 18R-LPSO phase on corrosion resistance of Mg−Zn−Y alloys [J]. Transactions of Nonferrous Metals Society of China, 2023, 33(2): 454−466.

[21] YIN Zheng, HE Ren-hua, CHEN Yang, YIN Zhou, YAN Kun, WANG Kun, YAN Hong, SONG Hong-gun, YIN Cheng-xin, GUAN Hong-yu, LUO Chao, HU Zhi, LUC C. Effects of surface micro–galvanic corrosion and corrosive film on the corrosion resistance of AZ91−*x*Nd alloys [J]. Applied Surface Science, 2021, 536: 147761.

[22] CAI Chang-hong, SONG Ren-bo, WANG Luan-xiang, LI Jing-yuan. Effect of anodic *T* phase on surface micro-galvanic corrosion of biodegradable Mg−Zn−Zr−Nd alloys [J]. Applied Surface Science, 2018, 462: 243−254.

[23] PENG Xiang, SUN Jia-wei, LIU Hong-jie, WU Guo-hua, LIU Wen-cai. Microstructure and corrosion behavior of as-homogenized and as-extruded Mg−*x*Li−3Al−2Zn−0.5Y alloys (*x*=4, 8, 12) [J]. Transactions of Nonferrous Metals Society of China, 2022, 32(1): 134−146.

[24] ZHANG Yuan-mi, WU Ya-xu, JIANG Yu-miao, WANG Li, ZHANG Jing-lai. Adsorbed film and synergistic effect of Benzyltriphenylphosphonium chloride and *L*-histidine for magnesium alloys corrosion in NaCl [J]. Journal of Alloys and Compounds, 2020, 849: 156230.

[25] LAMAKA S V, HOCHE D, PETRAUSKAS R P, BLAWERT C, ZHELUDKEVICH M L. A new concept for corrosion inhibition of magnesium: Suppression of iron re-deposition [J]. Electrochemistry Communications, 2016, 62: 5−8.

[26] GAO H, LI Q, DAI Y, LUO F, ZHANG H X. High efficiency corrosion inhibitor 8-hydroxyquinoline and its synergistic effect with sodium dodecylbenzenesulphonate on AZ91D magnesium alloy [J]. Corrosion Science, 2010, 52(5): 1603−1609.

[27] SU Hui-shuang, LIU Yue, GAO Xing, QIAN Ya-feng, LI Wei-jie, REN Tie-gang, WANG Li, ZHANG Jing-lai. Corrosion inhibition of magnesium alloy in NaCl solution by ionic liquid: Synthesis, electrochemical and theoretical studies [J]. Journal of Alloys and Compounds, 2019, 791: 681−689.

[28] FENG Zhi-yuan, HURLEY B, LI Ji-chao, BUCHHEIT R. Corrosion inhibition study of aqueous vanadate on Mg alloy AZ31 [J]. Journal of the Electrochemical Society, 2018, 165(2): 94−102.

[29] SEIFZADEH D, BEZAATPOUR A, JOGHANI R A. Corrosion inhibition effect of N,N′-bis(2-pyridylmethylidene)-1,2-diiminoethane on AZ91D magnesium alloy in acidic media [J]. Transactions of Nonferrous Metals Society of China, 2014, 24(11): 3441−3451.

[30] ZHOU Yu-xin, LU Xiao-peng, ZHELUDKEVICH M L, WANG Fu-hui. Tailoring corrosion and discharge performance of Mg anode by corrosion inhibitor [J]. Electrochimica Acta, 2022, 736: 141471.

[31] LU Xiao-peng, LI Yan, JU Peng-fei, CHEN Yan, YANG Jing-shuai, QIAN Kun, ZHANG Tao, WANG Fu-hui. Unveiling the inhibition mechanism of an effective inhibitor for AZ91 Mg alloy [J]. Corrosion Science, 2019, 148: 264−271.

[32] LI Yan, LU Xiao-peng, WU Ke-xin, YANG Lei, ZHANG Tao, WANG Fu-hui. Exploration the inhibition mechanism of sodium dodecyl sulfate on Mg alloy [J]. Corrosion Science, 2020, 168: 108559.

[33] YANG Jun-jie, BLAWERT C, LAMAKA S V , YASAKAU K A, WANG L, LAIPPLE D, SCHIEDA M, DI Shi-chun, ZHELUDKEVICH M L. Corrosion inhibition of pure Mg containing a high level of iron impurity in pH neutral NaCl solution [J]. Corrosion Science, 2018, 142: 222−237.

[34] XIAO T, DANG N, HOU L F, WEI Y H, GUO C L, DU H Y. Inhibiting effect of sodium lignosulphonate on the corrosion of AZ31 magnesium alloy in NaCl solution [R]. Rare Metal Materials and Engineering, 2016, 45: 1600−1604.

[35] DINODI N, SHETTY A N. Alkyl carboxylates as efficient and green inhibitors of magnesium alloy ZE41 corrosion in aqueous salt solution [J]. Corrosion Science, 2014, 85: 411−427.

[36] FENG Zhi-yuan, HURLEY B, ZHU Meng-lin, YANG Zi, HWANG J, BUCHHEIT R. Corrosion inhibition of AZ31 Mg alloy by aqueous selenite (SeO_3^{2-}) [J]. Journal of the Electrochemical Society, 2019, 166(14): 520−529.

[37] XU Rong-rong, JIANG Dian-xiao, ZHOU Yu-xin, LU Xiao-peng, ZHANG Tao, WANG Fu-hui. Influence of 2,6-dihydroxybenzoic acid on the corrosion behavior and discharge performance of AZ31 Mg alloy [J]. Vacuum, 2022, 200: 111031.

[38] UMOREN S A, ABDULLAHI M T, SOLOMON M M. An overview on the use of corrosion inhibitors for the corrosion control of Mg and its alloys in diverse media [J]. Journal of Materials Research and Technology, 2022, 20: 2060−2093.

[39] HSU W P, ZHONG Qi-ping, MATJEVIĆ E. The formation of uniform colloidal particles of magnesium fluoride and sodium magnesium fluoride [J]. Journal of Colloid and Interface Science, 1996, 181(1): 142−148.

[40] POKHAREL D B, WU Lin-ping, DONG Jun-hua, YADAV A P, SUBEDI D B, DHAKAL M, ZHA Lin, MU Xin, UMOH A J, KE Wei. Effect of glycine addition on the in-vitro corrosion behavior of AZ31 magnesium alloy in Hank's solution [J]. Journal of Materials Science & Technology, 2021, 81: 97−107.

[41] KHARITONOV D S, ZIMOWSKA M, RYL J, ZIELIŃSKI A, OSIPENKO M A, ADAMIEC J, WRZESIŃSKA A, CLAESSON P M, KURILO I I. Aqueous molybdate provides effective corrosion inhibition of WE43 magnesium alloy in sodium chloride solutions [J]. Corrosion Science, 2021, 190: 109664.

[42] PRINCE L, ROUSSEAU M A, NOIRFALISE X, DANGREAU L, COELHO L B, OLIVIER M G. Inhibitive effect of sodium carbonate on corrosion of AZ31 magnesium

alloy in NaCl solution [J]. Corrosion Science, 2021, 179: 109131.
[43] HUANG Dao-bing, HU Jun-ying, SONG Guang-ling, GUO Xing-peng. Inhibition effect of inorganic and organic inhibitors on the corrosion of Mg−10Gd−3Y−0.5Zr alloy in an ethylene glycol solution at ambient and elevated temperatures [J]. Electrochimica Acta, 2011, 56(27): 10166−10178.
[44] QIU You-min, TU Xiao-hui, LU Xiao-peng, YANG Jun-jie. A novel insight into synergistic corrosion inhibition of fluoride and DL-malate as a green hybrid inhibitor for magnesium alloy [J]. Corrosion Science, 2022, 199: 110177.

NaCl 溶液中 NaF 对 WE43 镁合金的缓蚀机制

杨云天 [1]，周钰昕 [1]，卢小鹏 [1]，马吉睿 [1]，杨俊杰 [2,3]，王福会 [1]

1. 东北大学 数字钢铁全国重点实验室，沈阳 110819；
2. 暨南大学 先进耐磨蚀及功能材料研究院，广州 510632；
3. 暨南大学 韶关研究院，韶关 512027

摘　要：采用 SEM、TEM、EPMA、XRD、XPS 和电化学测试等方法系统研究了 3.5% NaCl(质量分数)溶液中 NaF 对 WE43 镁合金显微组织、组成和腐蚀性能的影响。结果表明，NaF 是一种有效的 WE43 镁合金缓蚀剂。在中性 NaCl 溶液中，当 NaF 浓度为 40 mmol/L 时，抑制效率最高，其值为 92.6%。缓蚀剂与溶解的 Mg^{2+}发生反应，形成并沉积双层致密且具有保护性的腐蚀膜层，抑制了 WE43 合金的溶解。采用 FIB 和 TEM 分析了该双层腐蚀膜层的显微组织和组成。腐蚀膜外层主要由 $NaMgF_3$、MgF_2 和 MgO 组成，内层主要由 MgO 和 MgF_2 组成。

关键词：镁合金；腐蚀；腐蚀膜层；缓蚀剂；缓蚀机制

(Edited by Wei-ping CHEN)